

COVER PAGE

Document downloaded by @DAEL

Sat Nov 28 19:05:36 2026
For personal use

When automatic English translation is provided, only the original document is authentic.
The EAA cannot be held responsible of any translation error

Bibliographical reference

An Efficient Planar Inverse Acoustic Method Based on Toeplitz Matrices, J. W. Wind, M. H. M. Ellenbroek and A. De Boer, Acta Acustica **vol. 97** (Number 1), 2011, pp. 128-137

DOI
https://doi.org/10.3813/AAA.918393

ACTA ACUSTICA UNITED WITH ACUSTICA
Vol. 97 (2011) 128 – 137

DOI 10.3813/AAA.918393

An Efficient Planar Inverse Acoustic Method Based on Toeplitz Matrices

J. W. Wind, M. H. M. Ellenbroek, A. de Boer
University of Twente, Enschede, Netherlands. wind@microflown.com

Summary
This article proposes a new, fast method to solve inverse acoustic problems for planar sources. This problem is often encountered in practice and methods such as *planar nearfield acoustic holography* (PNAH) and *statistically optimised nearfield acoustic holography* (SONAH) are widely used to solve it. In this article, it is shown that the transfer matrix from an equidistant source grid to an equidistant field grid has a *Block Toeplitz with Toeplitz Blocks* (BTTB) structure. By using fast methods for BTTB matrices, the computational effort is reduced to a similar level as PNAH at an accuracy which is the same as SONAH. This is demonstrated in a case study, where computational time and the accuracy is compared. The accuracy is shown to be better than PNAH even if advanced sound field extrapolation techniques such as patch holography are used.

PACS no. 43.40.Sk, 43.60.Pt, 43.60.Sx

1. Introduction

Since an understanding of the causes of sound and vibration is vital in sound and vibration studies, inverse acoustical methods are important tools in this field. Successful applications can be found in tyre-road noise and car interior noise. The methods have also been applied to improve consumer appliances.

Inverse acoustical methods provide an approximation of the normal velocity at the surface of the source based on a measured sound field. The methods consist of the following steps (see Figure 1). Firstly, the acoustical pressure or particle velocity of the *sound field* is measured at a large number of field points close to the source surface. Secondly, the measured time data is represented in the frequency domain. Thirdly, the *forward model* is calculated. This model is represented by the transfer matrix from the noise source to each of the field points. Fourthly, the transfer matrix is inverted using *regularisation techniques* and multiplied by the processed measurement data. The result of an inverse acoustical calculation is the amplitude and phase of the source velocities.

The Rayleigh integral can be used to calculate the transfer matrix if the source is modelled to be an infinite plane. In the method discussed in this article, the transfer matrix is calculated based on a discretisation of the spatial domain, leading to an accurate forward model. The same approach is taken in the widely used method *statistically optimised nearfield acoustic holography* (SONAH) [1, 2]. A disadvantage of the existing algorithms for this purpose is the comparatively large amount of time and memory, especially if the inverse solutions are calculated for an entire frequency range. An advantage is its high accuracy.

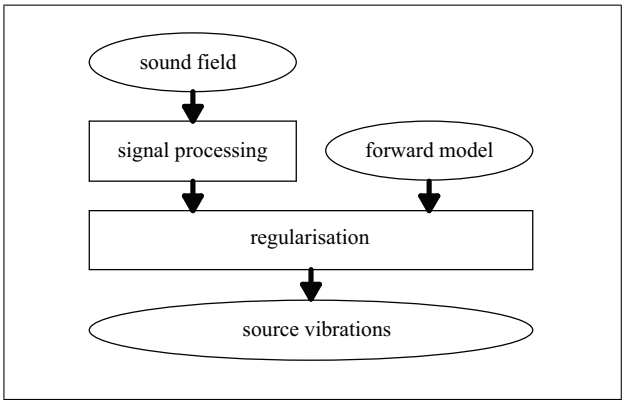

Figure 1. The steps required in inverse acoustics.

Planar Nearfield Acoustic Holography (PNAH) is an alternative to the numerical approach [3, 4]. It is based on the 2D spatial Fourier transform of the Rayleigh integral. To perform the inverse acoustic calculation, the 2D spatial Fourier transform is also applied to the field data, using the discrete Fourier transform (DFT). The Fourier transform of the source velocity is calculated using regularisation techniques and the inverse DFT is used to transform the source velocities into the spatial domain. In practice, the DFT is an inaccurate approximation of the continuous Fourier transform. To reduce the errors in the calculated source vibration, the sound field is extrapolated beyond the edges of the measured data (see also section 3). Nevertheless, the errors caused by the use of the discrete wavenumber domain can not be eliminated completely. This is

Received 26 April 2010,
accepted 3 August 2010.

© S. Hirzel Verlag · EAA

the largest disadvantage of PNAH. The advantage is the small computational effort which is required.

The approach proposed in this article is similar to SONAH. Both methods use the Rayleigh integral in the spatial domain to solve the inverse problem, but there are important differences. The new approach is more efficient, as shown in section 4. However, SONAH applies to sensors which are arranged in an arbitrary pattern whereas the current method is restricted to equidistantly spaced sensors. Although nearfield source localisation arrays usually consist of equidistantly spaced sensors, the current approach does not apply directly to nearfield source localisation using beamforming arrays whereas SONAH does.

This article is built up as follows. Section 2 introduces the new method and section 3 considers the basic theory of PNAH. A comparative study is performed in section 4 and conclusions are drawn in section 5.

2. The proposed method

2.1. Basic equations

The Rayleigh integral describes the pressure at field points $p(x_i)$, $i = \{1, 2, \cdots, M\}$ based on the normal velocities $v_n(\vec{y})$ at the source surface S. It is given by

$$p(\vec{x}_i) = 2\mathrm{j}\omega\rho_0 \int_S v_n(\vec{y}) G(|\vec{y} - \vec{x}|)\, \mathrm{d}S, \quad (1)$$

where $G(|\vec{y} - \vec{x}|) = \dfrac{\mathrm{e}^{-\mathrm{j}k|\vec{y}-\vec{x}|}}{4\pi|\vec{y} - \vec{x}|}$,

where ω, ρ_0 and j are the angular frequency, the density of air and the imaginary unit respectively.

The acoustical equations are discretised. The normal velocity at the source is approximated using a basis of functions $\mathrm{N}_j(\vec{y})$ with $\vec{y} \in S$ and $j = \{1, 2, \ldots, N\}$ such that the discrete form of the Rayleigh integral is [5]:

$$\mathbf{H}\mathbf{v} = \mathbf{p} \quad (2)$$

with
$$\begin{cases} p(\vec{x}_i) & = \mathbf{p}_i, \\ v_n(\vec{y}) & = \sum_j \mathrm{N}_j(\vec{y})\mathbf{v}_j, \\ \mathbf{H}_{ij} & = 2\mathrm{j}\omega\rho_0 \int_S \mathrm{N}_j(\vec{y}) G(|\vec{y} - \vec{x}_i|)\, \mathrm{d}S, \end{cases}$$

where $\mathbf{H} \in \mathbb{C}^{M\times N}$, $\mathbf{v} \in \mathbb{C}^N$ and $\mathbf{p} \in \mathbb{C}^M$ denote the *transfer matrix*, the *source vector* and *field vector* respectively.

To determine the source vector $\mathbf{v}$ based on the field vector $\mathbf{p}$, it is necessary to solve the matrix-vector equation (2) for $\mathbf{p}$. The transfer matrix is inherently ill-conditioned such that the least squares solution leads to incorrect results. *Regularisation methods* are used to find a suitable approximation.

2.2. The structure of the transfer matrix

This section shows that the transfer matrix $\mathbf{H}$ which follows from equation (2) has a Toeplitz structure under certain conditions. To simplify the figures and equations, a line source is studied in this section and the extension to a planar source is given in section 2.4. Furthermore, the structure shown here is under strict conditions and these conditions are widened in section 2.4.

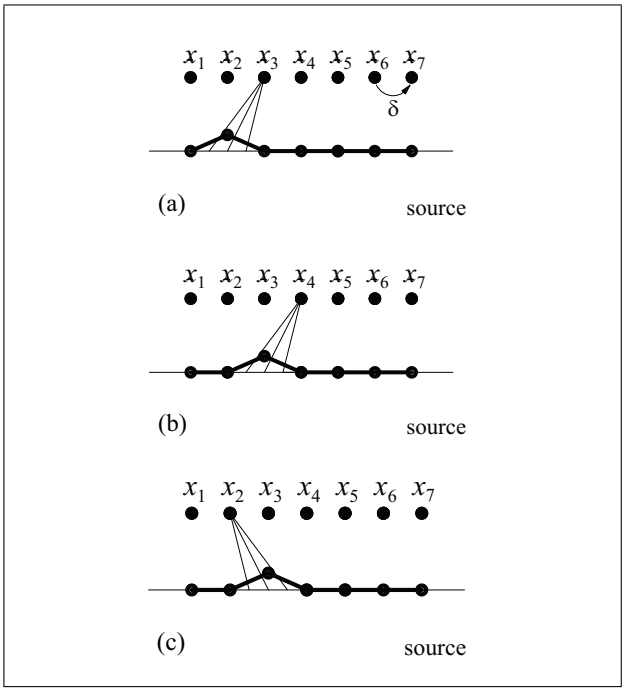

Figure 2. Graphical representation of the distances involved in three elements of the impedance matrix. Since the same distances are involved, the same value is obtained. (a) Distances for $\mathbf{H}_{23}$, (b) Distances for $\mathbf{H}_{34}$, (c) Distances for $\mathbf{H}_{32}$.

The field points are assumed to be located at equal distances δ along a line which is itself parallel to the source. Linear elements are used to discretise the source and it is assumed that each source node is located underneath a field point, such that the shape functions have the form indicated in Figure 2.

Using this discretisation, the integral in equation (2) can be regarded as a discrete form of a convolution. As can be seen in Figure 2, the same distances are involved in the calculation of $\mathbf{H}_{32}$, $\mathbf{H}_{43}$ and $\mathbf{H}_{23}$ such that the values of these elements of the transfer matrix are the same. It follows that it has the *Toeplitz structure*: $\mathbf{H}_{ij} = h_{i-j+1}$, and it is also symmetric $\mathbf{H}_{ij} = \mathbf{H}_{ji}$. Hence, the structure of the matrix is as follows.

$$\mathbf{H} = \begin{bmatrix} h_1 & h_2 & h_3 & \cdots & h_N \\ h_2 & h_1 & h_2 & \cdots & h_{N-1} \\ h_3 & h_2 & h_1 & \cdots & h_{N-2} \\ \vdots & \vdots & \vdots & \ddots & \vdots \\ h_N & h_{N-1} & h_{N-2} & \cdots & h_1 \end{bmatrix}. \quad (3)$$

The symmetric Toeplitz structure occurs for the case where the field data consists of velocities normal to the source plane. If the field data consists of velocities parallel to the source plane, then the matrix has a similar structure but it is skew-symmetric ($\mathbf{H}_{ij} = -\mathbf{H}_{ji}$).

Due to this Toeplitz structure, only the first column of the transfer matrix needs to be calculated and stored in

computer memory. Evidently, this reduces the computer power necessary to calculate the numerical integrals and to store the matrix in memory if the problem is large. The structure can also be used to solve the regularisation problem more efficiently by utilising the fast matrix-vector multiplication which is explained in the next section.

2.3. Fast matrix-vector multiplication

This section introduces a fast matrix-vector multiplication algorithm for Toeplitz matrices. This algorithm is well known in numerical mathematics but it has not been applied to inverse acoustics. The algorithm is applied to regularisation problems in section 2.5.

The matrix-vector multiplication algorithm is based on a circulant matrix $\mathbf{C} \in \mathbb{C}^{N\times N}$, which is a specific type of Toeplitz matrix,

$$\mathbf{C} = \begin{bmatrix} c_1 & c_N & c_{N-1} & \cdots & c_2 \\ c_2 & c_1 & c_N & \cdots & c_3 \\ c_3 & c_2 & c_1 & \cdots & c_4 \\ \vdots & \vdots & \vdots & \ddots & \vdots \\ c_N & c_{N-1} & c_{N-2} & \cdots & c_1 \end{bmatrix} \in \mathbb{C}^{N\times N}. \tag{4}$$

As in Toeplitz matrices, the matrix is structured such that $\mathbf{C}_{ij} = c_{i-j}$ for some sequence of numbers c_l, where $l \in \mathbb{Z}$ may be positive or negative. Contrary to Toeplitz matrices, any element that 'moves out of scope' on the right, 'moves into scope' on the left in the next row: $c_{l-N} = c_l$.

A matrix-vector multiplication with an $N \times N$ matrix commonly requires $O(N^2)$ operations but matrix-vector multiplication with a circulant matrix can be performed in only $O(N \log N)$ operations because all circulant matrices can be written in terms of their eigenvalue decomposition as follows:

$$\mathbf{C} = \mathbf{F}\mathbf{\Lambda}\mathbf{F}^{-1} \tag{5}$$

$$\text{where} \quad \begin{cases} \operatorname{diag}(\mathbf{\Lambda}) & = N\mathbf{F}^{-1}\mathbf{c}_1 \\ \mathbf{F}_{ij} & = \mathrm{e}^{-2\pi \mathrm{j}(i-1)(j-1)/N} \end{cases}$$

where $\mathbf{F}$ is termed the discrete Fourier transform matrix (DFT matrix) and $\mathbf{\Lambda}$ is the diagonal matrix with eigenvalues. The vector $\mathbf{c}_1 \in \mathbb{C}^N$ is the first column of $\mathbf{C}$. It can be seen that $\mathbf{\Lambda}$ is calculated from the first column of $\mathbf{C}$ directly.

It should be emphasised that equation (5) is an exact algebraic identity. A similar relation is used in PNAH but the relation used there is an approximation (see section 3) whereas equation (5) is exact for any grid size. Multiplication with a circulant matrix can be performed efficiently by implementing the following equation:

$$\mathbf{C}\mathbf{x} = \mathbf{F}\mathbf{\Lambda}\mathbf{F}^{-1}\mathbf{x} \tag{6}$$

where multiplications with $\mathbf{F}$ and $\mathbf{F}^{-1}$ are implemented as fast Fourier transforms (FFT) and the diagonal matrix $\mathbf{\Lambda}$ is calculated using the first column of $\mathbf{C}$. Since FFT algorithms require $O(N \log N)$ operations whereas a conventional matrix-vector multiplication requires $O(N^2)$ operations, the FFT-based approach is asymptotically faster. It is also more memory efficient becasue only the first column of $\mathbf{C}$ needs to be stored in computer memory.

This fast multiplication can be used for Toeplitz matrices as well. This is achieved by padding the Toeplitz matrix such that it becomes circulant:

$$\mathbf{C} = \begin{bmatrix} \mathbf{H} & \widehat{\mathbf{H}} \\ \widehat{\mathbf{H}} & \mathbf{H} \end{bmatrix} \in \mathbb{C}^{2n\times 2n}, \quad \text{where} \tag{7}$$

$$\widehat{\mathbf{H}} = \begin{bmatrix} 0 & h_N & h_{N-1} & \cdots & h_2 \\ h_N & 0 & h_N & \cdots & h_3 \\ h_{N-1} & h_N & 0 & \cdots & h_4 \\ \vdots & \vdots & \ddots & \vdots & \\ h_2 & h_3 & h_4 & \cdots & 0 \end{bmatrix} \in \mathbb{C}^{N\times N}, \tag{8}$$

where the diagonal terms of $\widehat{\mathbf{H}}$ are undetermined. The matrix-vector product $\mathbf{H}\mathbf{v} = \mathbf{p}$ can be calculated using the fast Fourier approach of equation (5), by writing:

$$\begin{bmatrix} \mathbf{H} & \widehat{\mathbf{H}} \\ \widehat{\mathbf{H}} & \mathbf{H} \end{bmatrix} \begin{Bmatrix} \mathbf{v} \\ 0 \end{Bmatrix} = \begin{Bmatrix} \mathbf{p} \\ \widehat{\mathbf{p}} \end{Bmatrix}, \tag{9}$$

where $\mathbf{p}$ is the required solution of the product and $\widehat{\mathbf{p}}$ is a nonphysical result that can be discarded. This use of the exact discrete identity is well known in the mathematical literature [6] as well as the literature on signal processing [7] but the use in inverse acoustics is new to the authors' knowledge.

2.4. Extension to practical problems

The algorithm of the previous section has been derived for the case where the number of source points is equal to the number of field points. However, the discretisation error in the forward model can be reduced by refining the source grid while keeping the field grid constant. Although the algorithm can not determine the pressure at just the field points, it can determine the pressure at all of the points located above a source point (see Figure 3). This set of points includes the field points. Since the points where no measurements have taken place are not relevant, their values are calculated but not used. Only the pressures at the field points are used in the inverse methods of section 2.5.

Another inaccuracy can be handled in the same way. The Rayleigh integral is based on a source in an infinite baffle, but the baffle is rarely present in acoustic experiments. This error can be alleviated by taking the source to be slightly larger than the field grid. This causes the transfer matrix to become rectangular but it can be treated in the same way as the case where the source grid is finer than the field grid. It is also depicted in Figure 3.

In practice, the source is two dimensional. This case can also be handled using the matrix-vector multiplication algorithm of section 2.3. For this purpose, the source nodes and the field points are both assumed to form an equidistant grid of $N_x \times N_y$ points and the node numbering is assumed to be column-by-column as depicted in Figure 3b. The resulting transfer matrix consists of $N_y \times N_y$ blocks of dimension $N_x \times N_x$. Each of the blocks has a Toeplitz

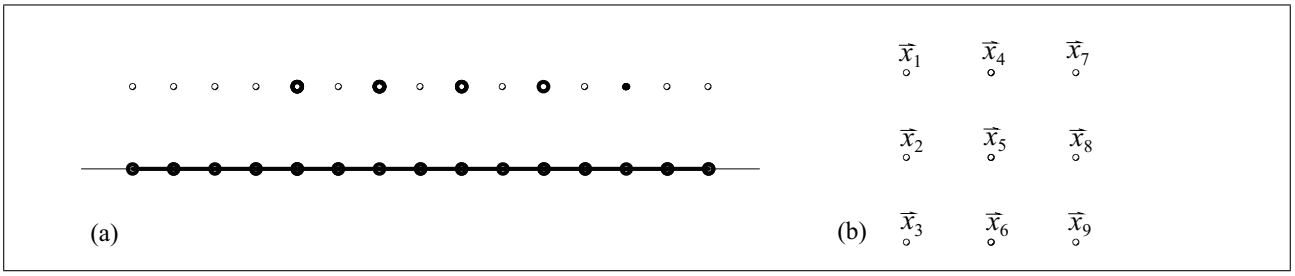

Figure 3. Extension to practical problems: finer source mesh and two dimensional source. (a) field points (∘), other points (·), (b) grid numbering.

structure and the blocks themselves also form a Toeplitz structure. This structure is known as block Toeplitz with Toeplitz blocks (BTTB). Each of the blocks can be extended to form a circulant matrix and the block structure itself can be extended to form a circulant block structure such that the fully extended matrix is block circulant with circulant blocks (BCCB). The fast matrix-vector multiplication can then be performed using a 2D FFT algorithm.

2.5. Regularisation

In the literature on numerical linear algebra, several fast algorithms are known to calculate the regularised inverse of a Toeplitz or BTTB matrix [6, 8]. This article considers Krylov subspace iteration methods such as conjugate gradients least squares (CGLS) or the least-squares QR (LSQR) method. The methods have originally been developed to solve systems of equations but they have an inherent regularising property: the first iteratands are oversmoothed but the smoothening decreases as the iteration continues. Since these methods are even attractive in applications where the Toeplitz structure does not occur, an abundance of literature is available on the implementation and the accuracy of the results [9, 10, 11].

The methods are especially attractive in the context of Toeplitz matrices because the matrix elements themselves are not used in the iterative process. Instead, only matrix-vector multiplications are used. These multiplications can be performed efficiently using the algorithm discussed in section 2.3.

A number of fast algorithms for Toeplitz matrices do not belong to the class of Krylov subspace methods. In recent years, researchers in applied mathematics and image processing have developed fast regularisation methods based on the *displacement rank* [8]. Although these methods are numerically efficient if the regularisation parameter is known, the methods are less efficient if the problem must be solved for many regularisation parameters.

Given the large number of articles on regularisation based on Toeplitz matrices, a comparison of various regularisation techniques is an attractive opportunity for research. However, the main goal of this article is to show that the Toeplitz structure is useful to calculate inverse acoustic solutions quickly and accurately. For this purpose, known inverse acoustical methods are compared to the Krylov subspace solver LSQR, where the matrix-vector multiplications are determined as explained in section 2.3.

3. PNAH

3.1. Introduction

Planar Nearfield Acoustic Holography (PNAH) has been proposed in 1985 by Maynard, Williams and co-workers [3, 4] based on earlier work by Graham (see [12]). It consists of the following steps. Firstly, the measured sound field is transformed to the spatial wave-number domain using the 2D Fourier transform. Since the measurement data consists of a finite number of points, the continuous Fourier transform (CFT) must be approximated by the discrete Fourier transform (DFT). To reduce the errors in this approximation, windowing and border-padding techniques are applied (see section 3.3). Secondly, an analytically known forward model is used to perform an inverse calculation in the wave number domain. Thirdly, the source vibrations are transformed into the spatial domain using the inverse DFT.

This section is built up as follows. Section 3.2 explains the basic equations for the case where the sound field is continuous and section 3.3 explains the case where the sound field consists of a finite number of points.

3.2. Solution in continuous space

The 2D spatial Fourier transform is defined to be

$$\tilde{f}(k_x, k_y) = \iint_{-\infty}^{\infty} f(x, y) \mathrm{e}^{-\mathrm{j}(k_x x + k_y y)} \,\mathrm{d}x \,\mathrm{d}y. \qquad (10)$$

It can be shown that the relation between the Fourier transformed normal velocity at the source $\tilde{v}_n(k_x, k_y)$ and the Fourier transformed pressure $\tilde{p}(k_x, k_y)$ is given by [13]:

$$\tilde{p}(k_x, k_y) = \overline{\rho_0 c_0 \frac{k}{k_z} \mathrm{e}^{\mathrm{j}k_z z}} \cdot \tilde{v}_n(k_x, k_y) \qquad (11)$$

with $\quad k_z = \sqrt{k^2 - k_x^2 - k_y^2}$

where $k = \omega / c_0$ and c_0 are the acoustic wave number and the speed of sound in the medium respectively. This expression is the complex conjugate of the expression in the reference work by Williams [13] because the angular frequency ω has the opposite sign in this article.

The inverse calculation consists of calculating the Fourier transformed normal velocity for each pair of wave numbers k_x, k_y. A filter function $\tilde{g}^{\alpha}(k_x, k_y)$ is applied to regularise the solution and α denotes the regularisation parameter.

$$\tilde{v}_n^{\dagger\alpha}(k_x, k_y) = \tilde{g}^{\alpha}(k_x, k_y) \cdot \overline{\frac{k_z}{k\rho_0 c_0} \mathrm{e}^{-\mathrm{j}k_z z}} \cdot \tilde{p}(k_x, k_y). \qquad (12)$$

Here, the superscript $(\cdot)^{\dagger\alpha}$ is used to show that regularisation has been applied. The solution in the spatial domain follows by applying the 2D inverse Fourier transform.

3.3. Discrete solution and extrapolation

The 2D discrete Fourier transform (2D DFT) is used to transform the measured sound field to the spatial wave-number domain. The field points are assumed to be located on an equidistant grid which is denoted (x_i, y_j) where i ranges from $-\frac{1}{2}N_x$ to $\frac{1}{2}N_x - 1$ and j ranges from $-\frac{1}{2}N_y$ to $\frac{1}{2}N_y - 1$. N_x and N_y are assumed to be even numbers. The 2D DFT has the following form:

$$\widetilde{p}(k_x, k_y) = \sum_{i=-\frac{1}{2}N_x}^{\frac{1}{2}N_x-1} \sum_{j=-\frac{1}{2}N_y}^{\frac{1}{2}N_y-1} p(x_i, y_j) \mathrm{e}^{-2\pi\mathrm{j}(k_x i/N_x + k_y j/N_y)} \qquad (13)$$

where the wave numbers k_x and k_y are chosen to form an equidistant grid in the wave-number domain. This grid can be chosen to consist of more points than the original set of field points, leading to an interpolation of the field data. In numerical implementations, this can be achieved by *zero padding*.

Replacing the spatial CFT with the DFT causes two types of error. *Aliasing* is caused by the fact that the sensors are too far apart. This error can not be attenuated using signal processing. *Leakage* is caused by the finite extent of the measured sound field. The DFT of the measured sound field is the same as the CFT of a a sound field which is extended periodically (see Figure 4a) [14].

Leakage can be reduced by adding fictitious field data beyond the edges of the measurement data (see Figure 4b). A straight-forward approach is *windowing and zero-padding*, where a spatial window is applied to the measurement data and the sound field is extended with zeros.

A more advanced sound field extrapolation technique is *Patch holography* [15]. The algorithm uses the following steps. First, an inverse computation is performed by extending the field data with zeros. Second, the sound field belonging to the computed source vibration is calculated. Third, the measurement data is extended using the calculated sound field. Fourth, an inverse computation is performed using the new extension of the sound field and steps 3-4 are repeated until convergence. Promising results have been achieved. The referred author has also applied the algorithm to a model which is based on a direct spatial discretisation, similar to SONAH, and he has achieved improved results. The main disadvantage of this algorithm is that the number of iterations required is so large that the required time is not competitive.

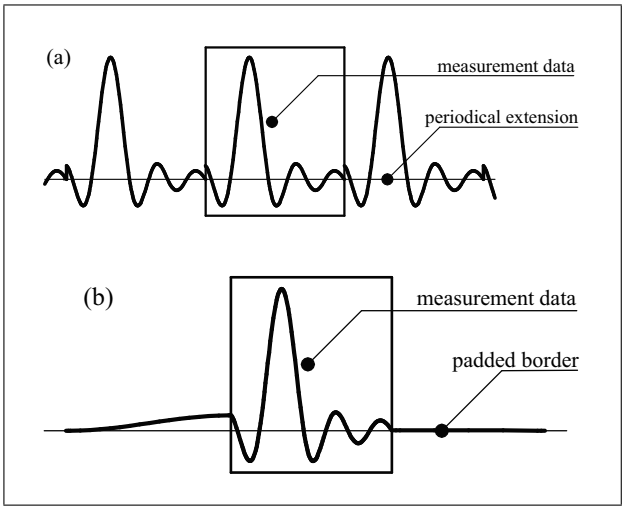

Figure 4. Sound field extrapolation. (a) Sound field and periodical extension, (b) Extrapolated sound field.

A sound field extrapolation technique which has been developed more recently is *linear predictive border-padding* (LPBP) [16]. The underlying concept is to extrapolate the sound field using autoregressive (AR) filters. The Burg method is used to compute an AR filter for each row of field points. This filter is then used to predict fictitious data beyond the known data points. The same procedure is applied along each column to extrapolate the field data along the other direction, leading to a smooth sound field along both extrapolation directions. A spatial window is applied to the extrapolated sound field. An advantage of this method is its speed.

4. Comparative study

4.1. Introduction

The new method has been developed to be more accurate than PNAH and faster than SONAH. The improved efficiency is especially important if the inverse calculation is performed for many frequencies and if the number of source and field points is large. This section applies various planar inverse acoustical methods to a numerical and experimental case study to compare their speed and accuracy. Section 4.2 compares the computation times and section 4.3 compares the accuracy of these methods.

The source that is used in this section and in the experimental validation is a hard-disk drive which is standing by for read or write operations. It is a rectangular box of $147 \times 102 \times 26$ mm (see Figure 5). The acoustic pressure is measured at a distance of 40 mm from the source surface and the field grid spans a rectangular area of 160×200 mm with a grid spacing of 10mm. The source grid extends 10mm beyond the field grid at all sides and bilinear quadrilateral elements of 0.5×0.5 mm are used such that the source grid consists of $73 \times 81 = 5913$ points. In the applications of PNAH, the sound field is extended to a grid of

128 × 128 points with a grid spacing of 10 mm. The computer used to compare the computation times is a 32bit 3G Hz PC with 1GB of RAM.

4.2. Computation time

The computation times are compared using the source and field grid of the experimental validation. It is also shown that the advantages of the new method are more pronounced for grids where the number of source points is a power of two and that the difference is larger in large scale problems than in small-scale problems.

The time required to form the forward model is compared first. The integration scheme which is used is an adaptive Gauss-Legendre quadrature [17]. This accurate but comparatively time-intensive integration scheme requires 75 ms to calculate the first column of the transfer matrix. The time required to calculate all elements of the transfer matrix directly is 26.8 seconds. In PNAH, the model is analytical and it is calculated in 10 ms.

The time necessary for PNAH methods depends on the implementation. A fast approach is to determine regularisation parameter based on the inverse solutions in the wave number domain instead of the spatial domain. This approach is faster because the inverse 2D Fourier transform does not have to be calculated for each regularisation parameter. A slower but more precise approach is to determine the regularisation parameter in the spatial domain. Although this requires an inverse 2D Fourier transform for each regularisation parameter, it makes it possible to study only the area below the sensors. The computation times of the faster method are more relevant because it is more common in practice. The slower approach is used in the next section to compare the accuracy of PNAH with other methods because the computed errors of PNAH would be unduly large otherwise.

The computation times are compared in Table I. Patch NAH is the slowest of all methods, requiring seven minutes and thirty seconds. The other PNAH methods require less than a second for the fast approach. These are the fastest methods that have been tested.

Table II (case A) compares the speed of SONAH and the new method. The most common way to perform Tikhonov regularisation for multiple regularisation paramters is by means of the SVD. The Matlab command SVD requires 10.6 seconds to decompose the transfer matrix and it is noted that the 'economy size' option has been used because it requires less computation time and memory. A way to solve the inverse acoustical problem without the fast matrix-vector multiplication is to use the Krylov subspace solver LSQR. It requires 3.9 seconds to complete. If the fast matrix-vector multiplications is applied, the time reduces to 2.4 seconds. In this case, the computation time is approximately two-thirds of the time required for the direct implementation.

As can be seen in Table II (case B), the advantages of the FFT-based matrix-vector multiplication are more pronounced if the source is chosen to be a grid of 64 × 64 points. The time required for the new method is reduced to 0.9 seconds compared to a computation time of 3.0 seconds for LSQR using the conventional matrix-vector multiplication. Hence, using the Block Toeplitz with Toeplitz Blocks structure reduces the computational time by roughly a factor of three in this case. It is also noted that the results of the 64 × 64 grid are as accurate as the results of the grid of 73 × 81 points.

The advantages of the new method grow as the number of source and field points increases. As can be seen in Table II (case C). In this case, the SVD can not be calculated due to limitations in the amount of accessible computer memory. For problems of a larger scale, the transfer matrix can not be stored in computer memory explicitly such that only the new method can be used. The time required for the new method using 128 × 128 source points and 64 × 64 field points is 25 seconds.

Given the three cases it can be concluded that PNAH using zero-padding, and LPBP are faster than the new approach but all other methods based on the spatial discretisation are slower. The new approach is especially attractive for large-scale problems, where the largest observed reduction in computation time is a factor of 6. It has also been shown that the new approach can perform inverse

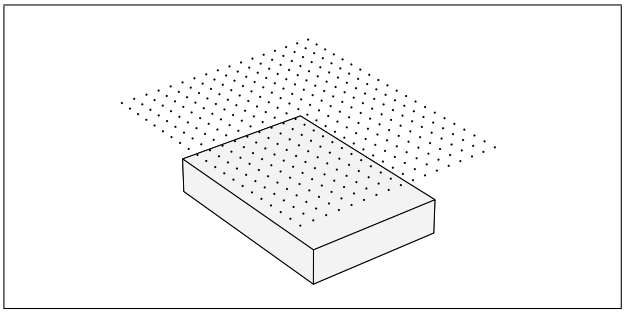

Figure 5. Field points and the geometry of the source.

Table I. PNAH: computation times.

	slow approach	fast approach
Source grid	128 × 128	128 × 128
Field grid	17 × 21	17 × 21
LPBP	2.6s	0.8s
Conventional BP	2.2s	0.4s
Patch NAH	450s	—

Table II. Numerical methods: computation times.

	A	B	C
Source grid	73 × 81	64 × 64	128 × 128
Field grid	17 × 21	17 × 21	32 × 32
SVD	10.6 s	7.8 s	—
Un structured Krylov	3.9 s	3.0 s	25.2 s
Toeplitz Krylov (new)	2.4 s	0.9 s	4.4 s

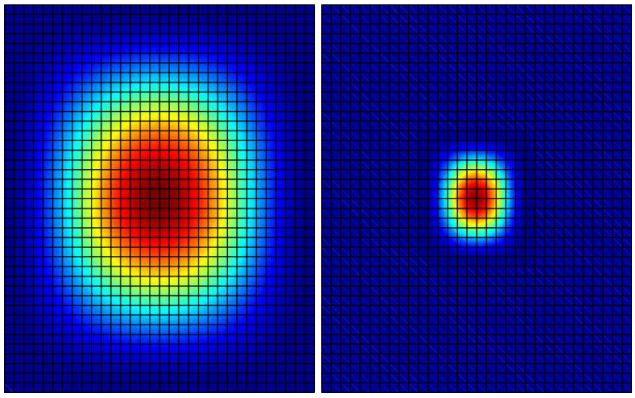

Figure 6. Source vectors used in the simulation study (absolute value). Left: Source A, 1075 Hz, right: Source B, 9669 Hz.

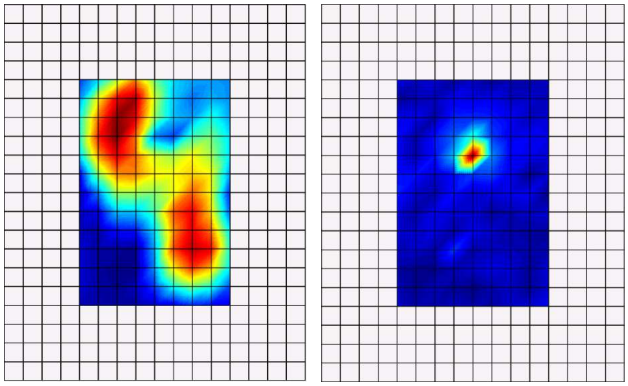

Figure 7. Laser vibrometer results of the experimental study (normal velocity, absolute value). Left: 1075 Hz, right: 9668 Hz.

calculations for problems where the transfer matrix is too large to be stored in computer memory.

4.3. Accuracy

This section compares the accuracy of the planar inverse acoustical methods by means of simulations and practical experiments.

In the simulation study, the sound field is calculated using the forward model of PNAH using a grid of 512 × 512 points and the relative error of the source vector is defined to be:

$$\epsilon_{rel} = \frac{\|\mathbf{v}^{\dagger\alpha} - \mathbf{v}\|}{\|\mathbf{v}\|} \tag{14}$$

where $\mathbf{v}^{\dagger\alpha}$ and $\mathbf{v}$ are the inverse result and the exact source vector respectively. The regularisation method used for the new method is LSQR and all other methods use Tikhonov regularisation. The inverse result is calculated for 90 regularisation parameters and the solution which has the smallest relative error is selected.

Two source vectors are used in the simulation study (see Figure 6). A smooth source vector is used at 1075 Hz and a spike-shaped source is used at the higher frequency of 9668 Hz. These frequencies are chosen because they have large responses in the experimental study such that a comparison between the simulation results and the experimental results is straightforward. A bar-chart of the errors is

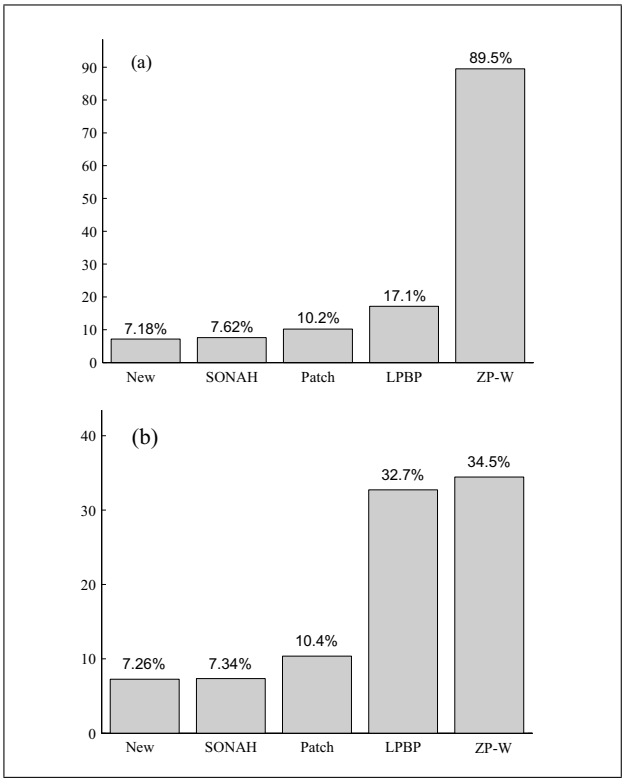

Figure 8. Errors found in the simulation study. (a) Source A, 1075 Hz, (b) Source B, 9668 Hz.

depicted in Figure 8. At 1075 Hz, the new method and SONAH are the most accurate, yielding errors within 8%. These methods are both based on the spatial discretisation. The worst result is achieved by PNAH using windowing and zero padding at an error of almost 90%. All other inverse solutions look similar (see Figure 9). For the simulation at 9668 Hz, the new method and SONAH have a relative error of 7.3%. Patch holography is close at 10.4% but PNAH using linear predictive border padding (LPBP) has an error of 32.7%. This large difference is caused by the fact that the extrapolated sound field is different from the actual sound field. Erroneous osscilations occur near the bottom and the top of the calculated source and the source is over smoothed to avoid the proliferation of these errors. LPBP requires the choice of an order of the filter. An order 4 filter has been used in all simulations and experiments which are shown in this article. The error can be reduced to 24,3% by choosing a filter of order 1 in this case. In both cases, the source can be distinguised clearly in Figure 9. Hence, it is concluded that the results of all methods, with the exception of windowing and zero padding, yield practically usable results.

Simulations have also been performed for various other sources and frequencies, the same trends are observed in these cases. If the vibrations at the source extend beyond the field grid, the errors are larger and the differences are small. All methods except windowing and zero-padding have been the most accurate for some source vectors and some frequencies.

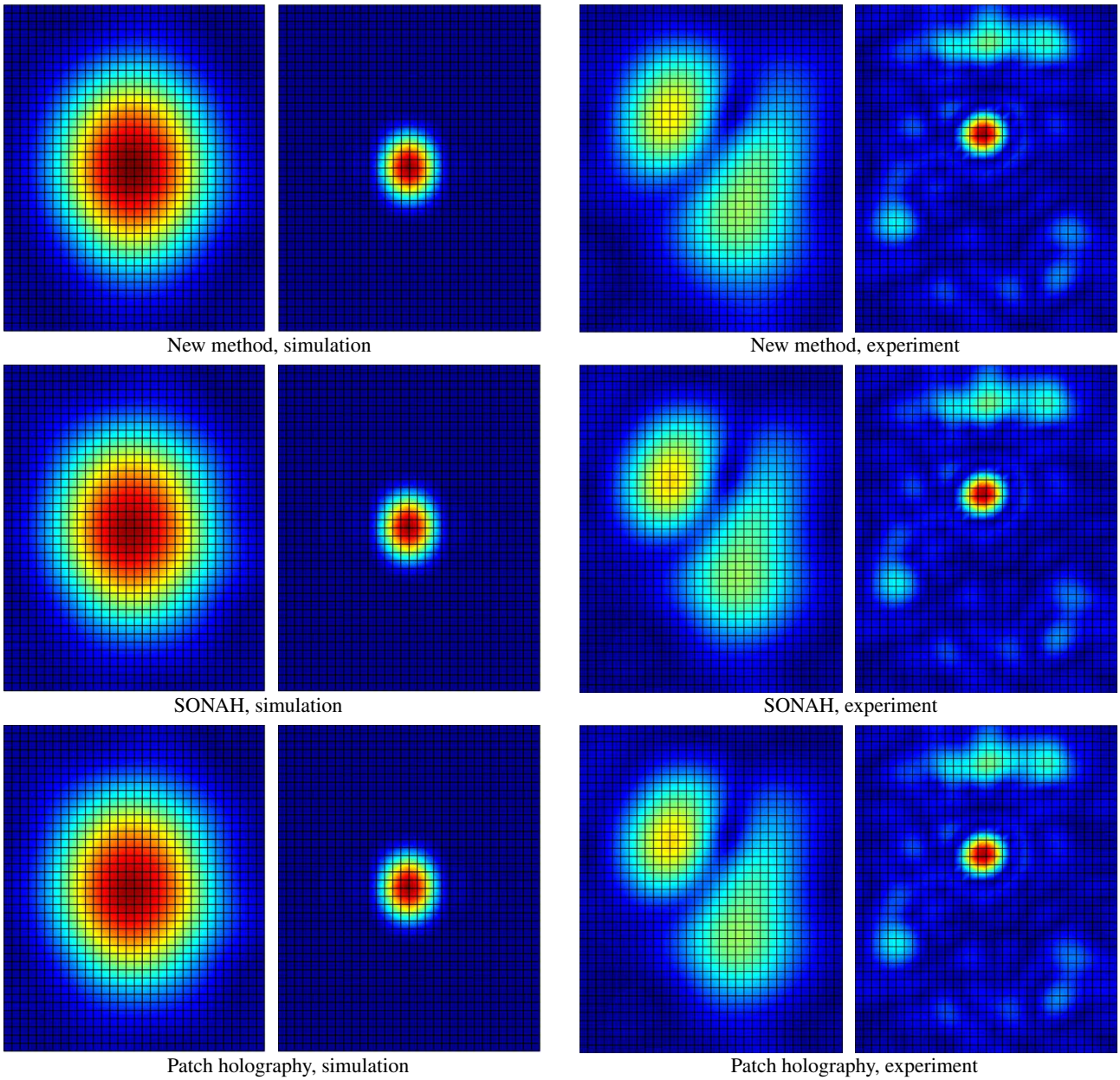

Figure 9. Inverse solutions the tested methods (absolute value). The results from left to right are (1) simulation of source A at 1075 Hz, (2) simulation of source B at 9669 Hz, (3) experiment at 1075 Hz (4) experiment at 9669 Hz. Continuation on next page.

Finally, measurement data from a hard disk drive are used to validate the methods in practice. The solutions are compared to laser vibrometer data (see Figure 7) and the regularisation parameter is chosen to be the point of maximum curvature of the L-curve [10]. Figure 9 depicts the results. As in the simulation study, the result of zero-padding is over-smoothed and all other results are similar. At 9669 Hz, the result of linear-predictive border-padding has a smaller amplitude and contains somewhat more noise than the other methods, but as in the simulation study, the point source can be seen clearly and all methods except windowing and zero-padding are considered to be practically useful.

Given the results of the simulations and the experimental validation, it is concluded that the new method has shown to be robust and as accurate as SONAH for the cases which have been studied. In the same cases, PNAH using LPBP has shown to be a faster method which is practically useful, though less accurate.

5. Conclusion

This article has proposed a new method for the planar inverse acoustical problem. The method makes use of the *Block Toeplitz with Toeplitz Blocks* (BTTB) structure of the transfer matrix to efficiently calculate solutions which are similar to other numerical methods such as SONAH. It has been shown that the advantages are especially large for large-scale problems and that the new method makes it possible to perform inverse calculations for problems where the transfer matrix is too large to be stored in the internal memory of the computer.

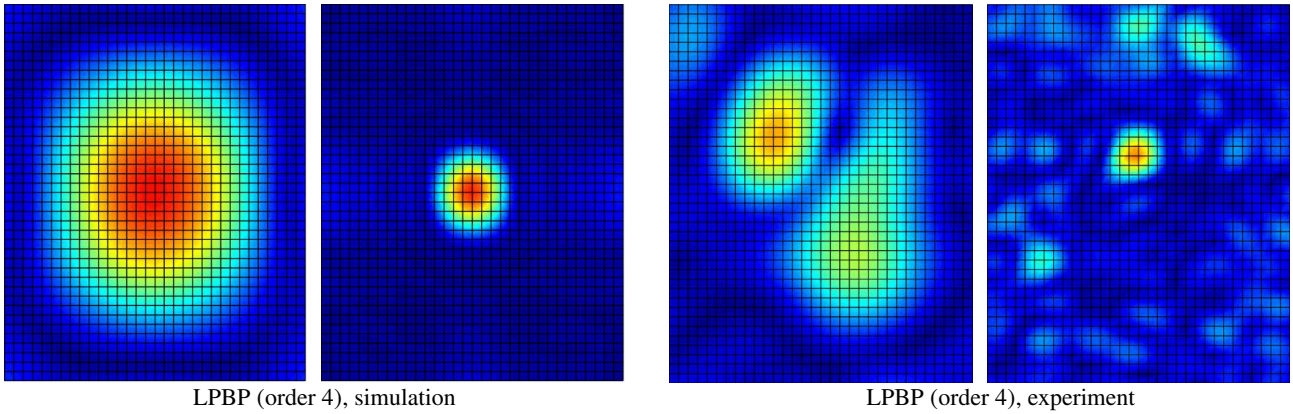

Figure 9. Continuation. Inverse solutions the tested methods (absolute value). The results from left to right are (1) simulation of source A at 1075 Hz, (2) simulation of source B at 9669 Hz, (3) experiment at 1075 Hz (4) experiment at 9669 Hz.

Although the new method is not as fast as planar nearfield acoustic holography (PNAH), the new method yields more accurate results. PNAH based on windowing and zero-padding yields results which are much less accurate than the other tested methods. The sound field extrapolation technique *linear predictive borderpadding* (LPBP) is competative in terms of speed and it yields results which are considered to be practically useful, but less accurate.

Acknowledgement

This work has been performed within the framework of project TWO.6618 of the Dutch Technology Foundation (STW).

Paul Taylor has provided a large number of textual improvements. His contributions are gratefully acknowledged.

References

[1] J. Hald: Patch near-field acoustic holography using a new statistically optimal method. Proceedings Inter-Noise 2003, Jeju Island, Korea, 2003, 2203–2210.

[2] R. Steiner, J. Hald: Near-field acoustical holography without the errors and limitations caused by the use of the DFT. Journal of Acoustics and Vibration **6** (2001).

[3] J. D. Maynard, E. G. Williams, Y. Lee: Nearfield acoustical holography: I. Theory of generalized holography and the development of NAH. Journal of the Acoustical Society of America **78** (1985) 1395–1413.

[4] W. A. Veronesi, J. D. Maynard: Nearfield acoustical holography (NAH) II. Holographic reconstruction algorithms and computer implementation. Journal of the Acoustical Society of America **81** (1987) 1307–1321.

[5] A. D. Pierce: Acoustics, an introduction to its physical principles and applications. third ed. Acoustical Society of America, 1994.

[6] P. C. Hansen: Deconvolution and regularization with Toeplitz matrices. Numerical Algorithms **29** (2002) 323–378.

[7] S. Haykin: Adaptive filter theory. second ed. Prentice Hall, 1991.

[8] K. Kimitei: Algorithms for Toeplitz Matrices with Applications to Image Deblurring. Diploma Thesis. Georgia State University, Atlanta GA, USA, 2005.

[9] G. H. Golub, C. F. V. Loan: Matrix computations. Third ed. Johns Hopkins University Press, Baltimore, 1996.

[10] P. C. Hansen: Rank-deficient and discrete ill-posed problems: Numerical aspects of linear inversion. Society for Industrial and Applied Mathematics, Philadelphia (PA), 1998.

[11] R. Visser: Regularization in nearfield acoustic source identification. Proceedings Eighth International Congress on Sound and Vibration, Hong Kong, China, 2001, 1637–1644.

[12] E. G. Williams, J. D. Maynard, E. Skudrzyk: Sound source reconstruction using a microphone array. Journal of the Acoustical Society of America **68** (1980) 340–344.

[13] E. G. Williams: Fourier Acoustics, Sound Radiation and Nearfield Acoustical Holography. first ed. Academic Press, 1999.

[14] D. B. Percival, A. T. Walden: Spectral analysis for physical applications. Cambridge University Press, 1993.

[15] E. G. Williams: Continuation of acoustic near-fields. Journal of the Acoustical Society of America **113** (2003) 1273–1281.

[16] R. Scholte: Fourier based high-resolution near-field sound imaging. Dissertation. Eindhoven University of Technology, Eindhoven, The Netherlands, 2008.

[17] R. Visser: A boundary element approach to acoustic radiation and source identification. Dissertation. University of Twente, Enschede, The Netherlands, 2004.